MANCHESTER 1824
The University of Manchester

The University of Manchester Research

Discontinuous yielding in wrought magnesium

DOI:
10.1016/j.commatsci.2017.02.010

Document Version
Accepted author manuscript

Link to publication record in Manchester Research Explorer

Citation for published version (APA):
Timár, G., Barnett, M. R., & da Fonseca, J. Q. (2017). Discontinuous yielding in wrought magnesium. *Computational Materials Science*, *132*, 81-91. https://doi.org/10.1016/j.commatsci.2017.02.010

Published in:
Computational Materials Science

Citing this paper
Please note that where the full-text provided on Manchester Research Explorer is the Author Accepted Manuscript or Proof version this may differ from the final Published version. If citing, it is advised that you check and use the publisher's definitive version.

General rights
Copyright and moral rights for the publications made accessible in the Research Explorer are retained by the authors and/or other copyright owners and it is a condition of accessing publications that users recognise and abide by the legal requirements associated with these rights.

Takedown policy
If you believe that this document breaches copyright please refer to the University of Manchester's Takedown Procedures [http://man.ac.uk/04Y6Bo] or contact uml.scholarlycommunications@manchester.ac.uk providing relevant details, so we can investigate your claim.

OPEN ACCESS

Download date:09. Dec. 2024

Discontinuous yielding in wrought magnesium

G. Timár[a,b,*], M.R. Barnett[c], J. Quinta da Fonseca[a]

[a] *Material Science Centre, University of Manchester, Manchester, M13 9PL, UK*
[b] *Departamento de Física da Universidade de Aveiro & I3N, Campus Universitário de Santiago, 3810-193 Aveiro, Portugal*
[c] *School of Engineering, Deakin University, Pigdons Rd., Geelong 3217, Australia*

Abstract

Recent reports of discontinuous yielding in the uniaxial compression of extruded magnesium suggest that twinning is accompanied by a significant stress decrease in the parent grain, leading to corresponding stress concentrations. We performed crystal plasticity finite element simulations using a simple twinning implementation that includes this "softening" effect for tensile twinning. With this method we were able to reproduce the experimentally observed yield point elongation and the Lüders-like propagation of strain and twinning over the sample. Twin variant selection was analysed in detail at various stages of deformation. Although lower rank variants were found to be activated, most of the twinning activity occurred on variants with the highest global Schmid factor. The stress fluctuations arising from the stress relaxation due to twinning did not appear to alter the dominance of the highest Schmid factor variant significantly. However, when twin softening is included, the twinning strain is dominated by a single variant. Despite giving rise to the highest stress fluctuations during yielding, simulations using the twin stress relaxation implementation actually showed less heterogeneity in stress after yielding. The results of our simple model suggest that "twin softening" could be key to the development of discontinuous yielding in extruded magnesium alloys.

Keywords: magnesium, Lüders, twinning, twin variant, discontinuous yielding, crystal plasticity

1. Introduction

Mechanical twinning plays an important role in the plastic deformation of magnesium and its alloys due to the limited number of easily activated independent slip systems. In most magnesium alloys, after

*Corresponding author
Email address: gtimar@ua.pt (G. Timár)

basal slip, tensile twinning on the $\{1\,0\,\bar{1}\,2\}$ plane is the deformation mode with the lowest critical resolved shear stress (CRSS). In many deformation conditions, e.g. compression in the sheet plane of rolled sheet or compression along the extrusion direction in an extrusion sample, tensile twinning is responsible for the majority of plastic strain at low applied strains [1, 2, 3]. Under these conditions, twinning is expected to significantly affect yielding and immediate post-yielding behaviour. A sound understanding of the deformation of magnesium alloys requires, therefore, an accurate picture of how tensile twins nucleate and propagate. The twinning behaviour at yielding will strongly influence the stability of deformation at later stages. Macroscopically, it will affect the work hardening rate which determines uniform elongation in tension. Microscopically, twins play a part in introducing local stress heterogeneities, which might limit ductility during biaxial deformation.

In this article we use a crystal plasticity finite element framework to investigate the effect of twinning on the development of local deformation and stress heterogeneity during plastic deformation of magnesium. The aim is to explore the effects of relative twin to slip activity and the possible effects of a "softening" rule for twinning.

Twin variant selection can be used as an indicator of the magnitude of stress fluctuations present in the material during plastic deformation, caused by the interaction of elastically and plastically anisotropic grains. Experimental studies of twin variant selection generally rely on the statistical analysis of EBSD data. In [4, 5, 6, 7, 8] large deviations were found from the twinning behaviour expected from simple Schmid factor considerations. An extreme example of such deviations is [4], where a magnesium AZ31 rolled sample was compressed to 5% along the transverse direction. No relationship was found between the observed volume fraction of a twin variant and the Schmid factor of the given variant. In [5] high-purity zirconium was deformed under similar conditions. Strong non-Schmid behaviour was found for twin nucleation and almost no correlation for twin thickness and Schmid factor. In contrast, Barnett et al. [1, 9] have recently reported "well-behaved" tensile twinning in a detailed statistical analysis of EBSD data obtained from the uniaxial compression of an extruded magnesium AZ31 sample along the extrusion direction. This difference in the twinning behaviour could be caused partly by the difference in microstructure: "well-behaved" twinning was observed for fine grained specimens (mean grain size of $\approx 10\mu m$) whereas the strong non-Schmid twinning behaviour was mainly observed for coarser grains and a wider distribution of grain sizes. Wider

grain size distributions will probably cause higher stress fluctuations at grain boundaries, leading to stronger deviation from the behaviour expected from Schmid factor considerations. An example of the importance of grain sizes and grain boundary irregularity can be seen in [10] where crystal plasticity finite element (CPFE) simulations systematically underestimate the non-Schmid behaviour of tensile twinning observed in the experiments. CPFE models are likely to provide more accurate predictions for fine grained materials and narrow grain size distributions.

Recently, Lüders-like deformation and the corresponding yield point elongation have been reported in [2, 3] for fine grained AZ31 and ZM20 magnesium alloys. It is suggested that the cause of this phenomenon is the stress relaxation occurring in twinned grains, and the consequent concentration of stress at the twin tips. These stress concentrations lead to a higher probability of twin nucleation in neighbouring grains. This twin triggering effect is believed to be responsible for the Lüders-like propagation of deformation and twinning. This explanation assumes that once a twin nucleates, the growth of the twin occurs at a lower stress. Recent modelling work has shown that softening is important to the formation of twin bands in single crystals and to the propagation of twinning between neighbouring grains with high misorientations [11]. Twin softening provides the local stress drop, analogous to dislocation unpinning in steels, that is required for Lüders-like yielding [12, 13, 14, 15, 16].

In recent years, the EPSC model [17] has been used to successfully predict macroscopic stress-strain behaviour [17, 18, 19, 20] and certain aspects of lattice strain evolution [18, 19] in magnesium, while the VPSC model [21] has proved successful in predicting texture evolution [21, 22, 23, 24, 25] and twin volume fraction [22, 25]. Although these mean field models have proved capable of accounting for many important aspects of deformation, they lose their validity when the phenomena in question depend significantly on local fluctuations of stress and strain. In such situations full field models have a clear advantage, even though the numbers of grains considered are generally lower due to the increased computational cost.

In this work we employ a crystal plasticity finite element model (CPFEM) to study the role of basal slip and twinning in the yielding behaviour of extruded magnesium in uniaxial compression. We implement a stress relaxation rule for tensile twinning and analyse its influence on the stress heterogeneity during and after yielding. We present a thorough analysis of twin variant selection, discussing in detail the effect of twin stress relaxation on stress fluctuations that determine how plastic strain is distributed among the different

deformation modes. Further, we aim to investigate to what extent the experimental observations related to Lüders-like propagation can be reproduced by assuming twin stress relaxation in our model.

2. Model construction

We simulate the deformation in polycrystalline magnesium using a three-dimensional elasto-viscoplastic CPFE model that has previously been used to successfully predict texture evolution and intergranular stresses in interstitial free steel [26, 27] and which we have also used to model the effect of texture on twin clustering [28] and to study the effect of solute content on twinning in Zr alloys [29]. A detailed description of the solution algorithm - in the context of the initial, two-dimensional version of the model - can be found in [30]. The model uses a small strain finite element implementation, i.e. based on infinitesimal strain theory. This is probably a valid choice considering the small overall strains simulated (up to 2%) and the large number of strain increments used (4000).

In this model, plastic deformation is assumed to occur by slip and twinning according to

$$\frac{\dot{\gamma}}{\dot{\gamma}_0} = \left(\frac{\tau}{\tau_0}\right)^{1/m} \tag{1}$$

where $\dot{\gamma}$ is the shear rate, τ the resolved shear stress and τ_0 the CRSS for any given slip/twin system. The rate sensitivity has the value $m = 0.02$ for all slip/twin systems. Focusing our study on relatively low strains, we have neglected hardening, i.e. τ_0 remains the same for all slip systems throughout the simulations. This significantly reduces the number of parameters in the model.

In the model twinning is considered only as a kind of unidirectional slip, i.e. twin systems are considered to be slip systems on which shear can occur only in one direction - determined by the twinning geometry. This is similar to the way twinning is modelled in the EPSC approach (e.g [18]).

The objective is to simulate elasto-plastic yielding and the early stages of plastic deformation, at which stage twins are still mostly very thin structures and the twinning volume fraction is small. It is reasonable to assume that, at this early stage, the effect of twins is mainly to contribute additional shear modes and that the effects of the lattice reorientation are only secondary.

During tensile twinning, it is assumed that propagation occurs at lower stresses than nucleation, then twinning relaxes the stresses in the twinned grains, whilst increasing the stresses in the neighbouring grains.

To model this twin softening behaviour, the CRSS of an active twin system is lowered according to:

$$\tau_t^c(\gamma) = (\tau_1^c - \tau_2^c)e^{-\gamma/g} + \tau_2^c \tag{2}$$

where γ is the accumulated shear on the given twin system and g is the scale parameter of the decay-law. τ_1^c and τ_2^c are the initial and asymptotic CRSS values for twinning.

We used $g = 2 \times 10^{-5}$ in all our simulations. As we will demonstrate, the simulation results show very little sensitivity to the value of this scale parameter. The effect of this "softening law" is to lower the stresses in the parent grain by allowing the deformation to occur by twinning at a lower stress.

The elastic compliance tensor elements used in the simulations were those of magnesium single crystal: $S_{11} = 22 \times 10^{-6}, S_{33} = 19.7 \times 10^{-6}, S_{44} = 60.98 \times 10^{-6}, S_{12} = -7.75 \times 10^{-6}, S_{13} = -4.96 \times 10^{-6}$, all in units of MPa^{-1}. The values were obtained from literature [31].

3. Simulations

All simulations were carried out on a cubic volume under uniaxial compression up to 2% strain. 20 node isoparametric brick elements were used in all cases, each element containing 8 integration points (IPs). The simulated polycrystal consisted of $10 \times 10 \times 10 = 1000$ elements, i.e. 8000 IPs. The starting texture was a simulated extrusion texture (Fig. 1), which was obtained by simulating the deformation of a homogeneous random textured initial sample in uniaxial tension until the distribution of the angle between c-axis and ED matched that measured in [9].

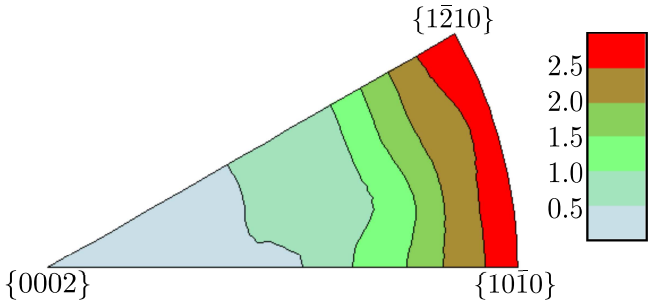

Figure 1: Initial texture used in all simulations. Reference direction is ED (X direction in the simulation coordinate system.)

In the simulations, the loading direction was always ED, which corresponds to the X direction in the simu-

CRSS values (MPa)	basal slip	prismatic slip	tensile twinning
Simulation A	15	75	45
Simulation B	15	75	15
Simulation C	15	75	$45 \rightarrow 15$

Table 1: CRSS values for the slip/twin modes used in the simulations. Values are given in MPa. Simulations *A* and *B* had constant CRSS values for twinning, while in Simulation *C* it was reduced from 45 MPa to 15 MPa, according to Eq. (2).

lation coordinate system. Only basal slip, prismatic slip and $\{1\,0\,\bar{1}\,2\}\,\langle\bar{1}\,0\,1\,1\rangle$ tensile twinning were considered. Pyramidal slip was neglected, as it is not expected to contribute significantly to deformation at the low strains considered in this study, due to its markedly higher CRSS.

In order to separate the effects of intergranular interactions and intragranular heterogeneity, we performed two sets of simulations: *Set 1*, where each IP corresponded to a separate orientation, i.e. different grain, and *Set 2*, where a whole element (consisting of 8 IPs) corresponded to a grain.

In each of the two sets, we performed three simulations: simulation *A*, where twinning is difficult with respect to basal slip, *B* where the CRSS for twinning is equal to that for basal slip and *C* the twinning CRSS starts off at the same value used in *A* and then drops to the value used in *B* according to Eq. (2). The CRSS for prismatic slip is the same in all simulations and higher than that of basal slip and twinning. The CRSS values used are given in Table 1.

4. Results

4.1. Macroscopic behaviour

The macroscopic stress-strain responses obtained for the simulations are shown in Figure 2. The observed hardening, in the absence of "constitutive" hardening, is entirely due to the elastic-plastic transition and the strong plastic anisotropy. Whilst some grains deform plastically, others deform only elastically producing the high work hardening region just after yield. There is also a small amount of work hardening, even after a strain of 0.01. This is caused by the difference in strain rates in the differently oriented grains. After an initial elastic region (Stage I) all simulations show micro-yielding by basal slip (Stage II), followed by yielding by tensile twinning (Stage III). (Prismatic slip, having the highest CRSS, also occurs in Stage III.) Additionally, simulation *C* in both sets exhibits an upper yield point followed by a yield plateau after which the flow stress approaches that of simulation *B*. *Set 2, C* exhibits a slightly flatter, more elongated

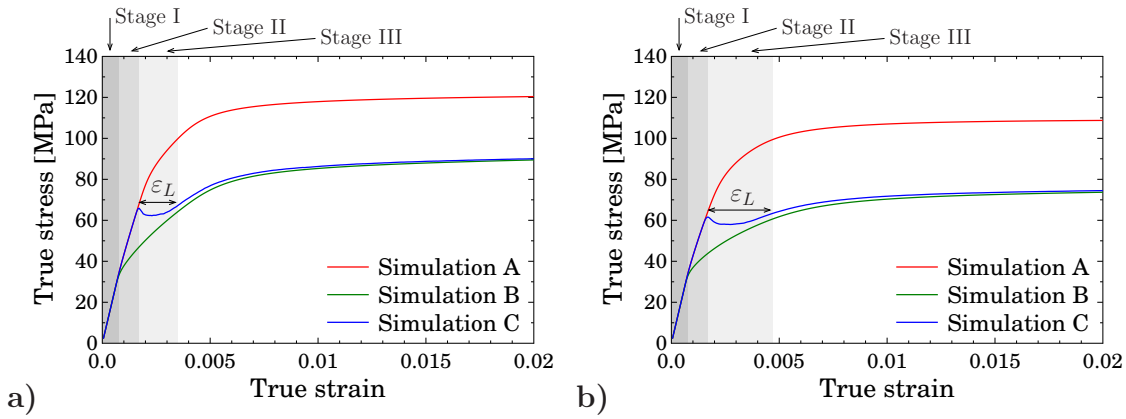

Figure 2: Stress-strain curves for all three simulations in Set 1 *(a)* and Set 2 *(b)*. Yield elongation is shown denoted by ε_L in both cases. Stage I: elastic region, Stage II: basal slip region, Stage III: tensile twinning region.

yield plateau than *Set 1, C*. It is clear that the introduction of twin softening introduces a yield plateau, which can be quantified by ε_L, defined as the difference in applied strain at the yield, and at the point at which the flow stress recovers to that at yield. Further, we performed simulations where g was varied in a wide range, keeping all other parameters of simulation *Set 2, C* constant. The resulting stress-strain curves from these simulations can be seen in Fig. 3 with the dependence of the yield elongation ε_L on g shown in the inset. Evidently, varying g over almost two orders of magnitude only has a very small effect on the yield elongation. The exact dependence of correlation length and yield elongation on the CRSS drop and the value g is beyond our scope. Here we chose a value that produces yield elongations in order to study the stress distributions and twin variant selection under such conditions.

The von Mises strain along the gauge is shown in Fig. 4 during yield. The maps show that whereas for simulations *A* and *B* yield happens at scattered locations along the gauge, simulations *C* develop a yield front, which propagates during yielding. This effect is more pronounced in *Set 2* than *Set 1*, which implies that the propagation is enhanced by intergranular heterogeneity. From here on, we concentrate only on *Set 2*, as these simulations are likely to be more realistic in terms of modelling the stress fluctuations during the elastic-plastic transition.

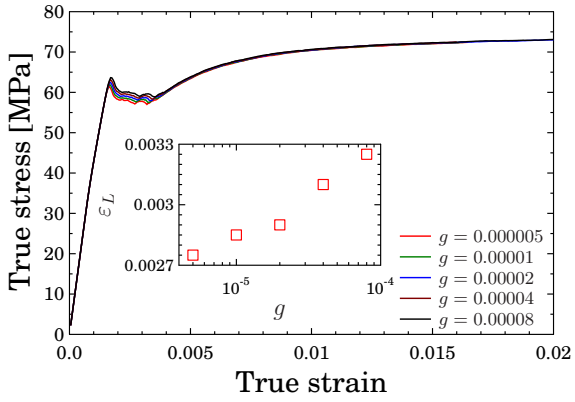

Figure 3: Stress-strain curves for different values of the decay scale parameter g. Inset: dependence of yield elongation on g.

4.2. Diffraction elastic strains

In-situ diffraction experiments have been used to study the yield behaviour of magnesium [2, 18, 19, 32, 33, 34], the interpretation of which requires polycrystalline deformation modelling. The EPSC model has been extensively used to predict lattice strains in magnesium under various deformation conditions [2, 18, 19, 33, 34]. In situations where deformation is mostly homogeneous, the EPSC model can provide good fits to the measured lattice strains [18, 19]. However, in some cases like, for example, in [2], the EPSC cannot fit the diffraction elastic responses. This was attributed to the kind of heterogeneous deformation our twin relaxation model produces. To see if accounting for twin relaxation impacts significantly on lattice strain predictions, we analysed the axial and radial lattice strains (Fig. 5) calculated for the following 6 plane families: $\{0\,0\,0\,2\}$, $\{1\,0\,\bar{1}\,0\}$, $\{1\,0\,\bar{1}\,1\}$, $\{1\,1\,\bar{2}\,0\}$, $\{2\,0\,\bar{2}\,1\}$ and $\{1\,0\,\bar{1}\,3\}$ during yield.

Although both the EPSC results [2] and our predictions make good approximations to the axial lattice strains measured in the experiments, only the CPFEM predicts the sudden strain reversal in $\{0\,0\,0\,2\}_{\perp}$ and $\{1\,0\,\bar{1}\,3\}_{\perp}$ grain families, along the transverse direction. Simulation *C* captures the effect very well, implying that the stress relaxation assumed for twinning in our model is, in a mesoscopic average sense, a good approximation of the actual phenomenon. Simulations *A* and *B*, without the stress decay rule, do not show a drastic strain reversal. In a recent article, Mareau and Daymond [35] proposed a new micromechanical model which attempts to account for the strain and stress gradients generated by twinning. This model is also capable of capturing the transverse strain reversal observed during in-situ straining diffraction experiments

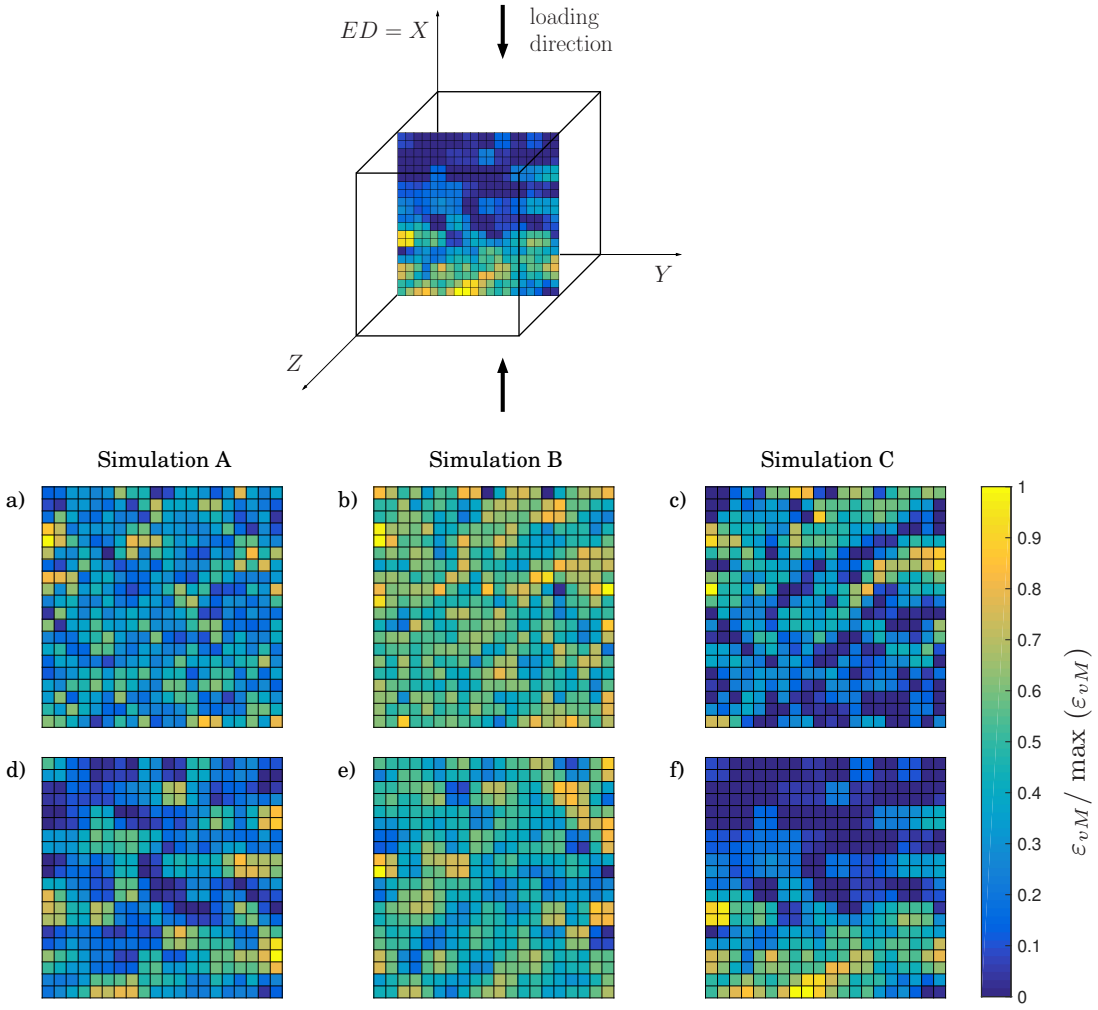

Figure 4: Maps of von Mises equivalent strain for the XY plane cross section (see schematic diagram) for all three simulations in Set 1 *(a, b, c)* and Set 2 *(d, e, f)*. For simulations *A* and *B* yield happens at scattered locations, while simulations *C* develop a yield front, which propagates during yielding. This is particularly apparent in *f* Set 2, simulation C. The applied strains in all cases were chosen so that the fraction of twinned IPs is the same (≈ 0.16), to allow for a meaningful comparison of how strain heterogeneity is influenced by twinning. The strain values were normalized by the maximum von Mises strain value in the given map, as these values varied considerably. The maximum von Mises strain values ($\max(\varepsilon_{vM})$) were *(a)* 0.0038, *(b)* 0.0013, *(c)* 0.004, *(d)* 0.0055, *(e)* 0.0015 and *(f)* 0.0056. The applied strains ($\langle\varepsilon_{xx}\rangle$) were *(a)* 0.0032, *(b)* 0.0016, *(c)* 0.0023, *(d)* 0.0032, *(e)* 0.0015 and *(f)* 0.0024. (For comparison the same regions are shown at the same applied strains in Fig. 8.)

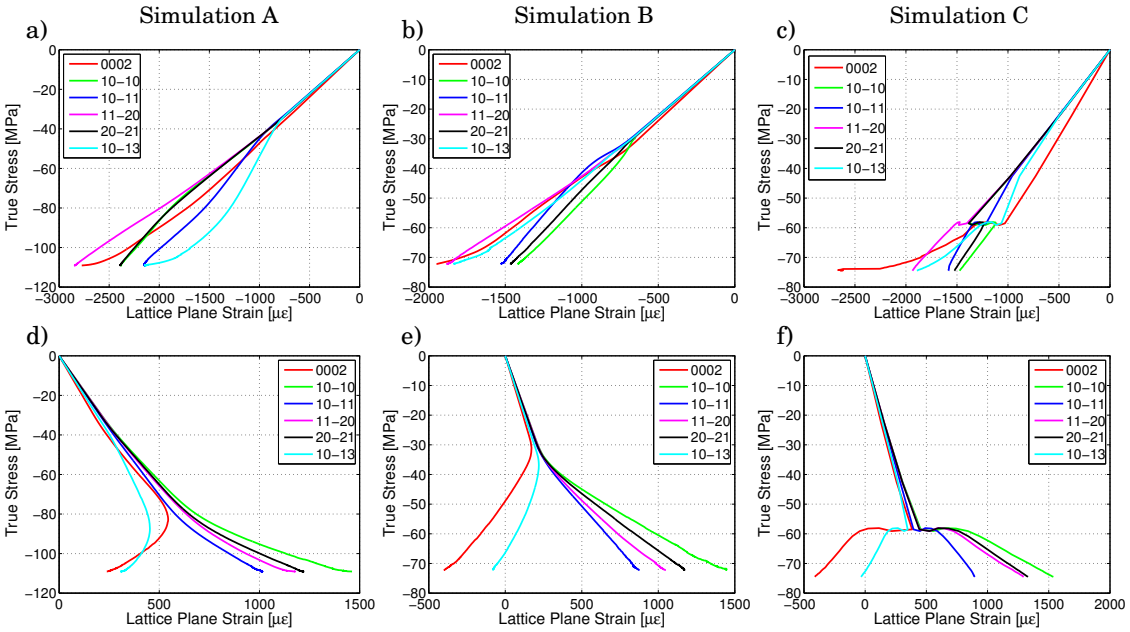

Figure 5: Axial *(a, b, c)* and radial *(d, e, f)* lattice strains.

and, crucially, their model also includes twin softening. Our results suggest that the success of their model owes more to the latter than to the new strategy proposed for partitioning the stress and strain fields between twinned and untwinned domains. The model used here treats twinning as a pseudo-slip system in the usual viscoplastic crystal plasticity formulation and not only predicts the $\{1\,0\,\bar{1}\,0\}_{\perp}$ and $\{1\,0\,\bar{1}\,1\}_{\perp}$ transverse responses well, it also predicts the complementary inflection in the $\{0\,0\,0\,2\}_{\perp}$ family.

4.3. Twinning activity and variant selection

The evolution of twinning activity with applied strain is shown in Fig. 6 (a). Twinning frequency is defined as

$$F_t = \frac{1}{N}\frac{d\Gamma(\varepsilon)}{d\varepsilon} \tag{3}$$

where N is the number of IPs and $\Gamma(\varepsilon)$ is the cumulative number of twin initiations in the entire system, as a function of applied strain. The plots show that twinning starts early in simulation *B* because of the low CRSS. In this case, the twinning frequency quickly reaches a very high maximum and drops almost as

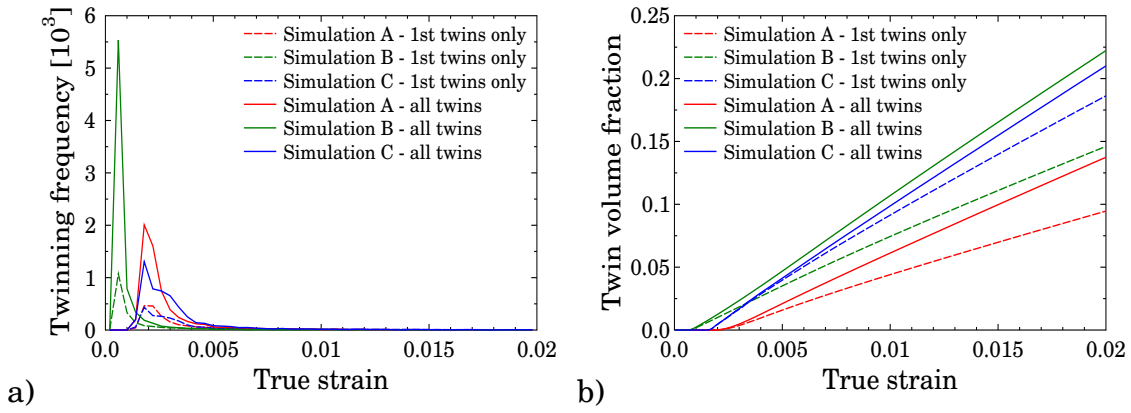

Figure 6: *(a)* Twin initiation frequency F_t (see Eq. (3)) and *(b)* twin volume fraction, as functions of applied strain.

quickly, although the twinning rate drops more slowly at higher strains.

In simulations *A* and *C*, twinning starts later, and the maximum twinning frequency values attained are lower than those in *B* . Twinning frequencies for these two simulations are almost identical up to a strain of ≈ 0.0017, when twinning frequency for simulation *C* drops sharply at first and then more slowly. This corresponds to the stress drop - the beginning of the yield elongation region - in the global stress-strain curve. In simulation A, the maximum twinning frequency is higher and the subsequent drop in twin activity is faster: twin initiation stops at ≈ 0.003, whereas it continues until ≈ 0.004 in simulation *C*.

The twinning frequency for the first twin variant is also plotted in Fig. 6 (a). Its evolution is similar to the overall twinning frequency but the different variants will make different contributions to the total twinning strain. To assess their relative contribution, the twin volume fraction is plotted as a function of applied strain in Fig. 6 (b). Twin volume fraction is defined as the average accumulated twinning shear per IP, divided by 0.13, the characteristic twinning shear for the $\{1\,0\,\bar{1}\,2\}\,\langle\bar{1}\,0\,1\,1\rangle$ tensile twin in magnesium. The dependence of twin volume fraction on strain is approximately linear in all cases. Simulations *B* and *C* attain higher twin volume fractions (≈ 0.22 by 0.02 applied strain) than simulation *A* due to their lower twin CRSS (asymptotic CRSS in the case of simulation *C*). Importantly, in simulation *C* the overall twinning shear is borne almost entirely by first variant twins in IPs. This corresponds to most grains showing only one active variant.

Finally, we are interested in the distribution of twin variants for the different simulations. Comparison of variant rank distributions obtained in our simulations to experimental ones provides valuable information

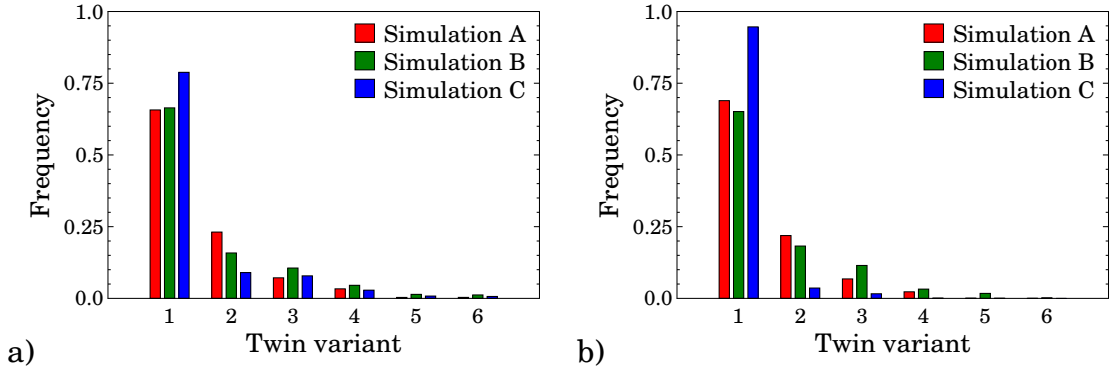

Figure 7: Twin variant rank distributions. *(a)* Based on global Schmid factor, *(b)* based on local Schmid factor.

regarding the nature of the developing stress field during yielding and of the validity of our twin relaxation assumption.

Figure 7 shows twin variant rank distributions based on global Schmid factor (a) and local Schmid factor (b). In calculating the distributions active variant ranks were weighted by the total accumulated twinning shear on the given variant. Our definition of the Schmid factor was as follows:

$$SF = RSS/||\sigma|| \tag{4}$$

where RSS is the resolved shear stress. $\sigma = \sigma_{global}$ for the GSF (global Schmid factor) and $\sigma = \sigma_{local}$ for the LSF (local Schmid factor). The norm used here is the maximum absolute eigenvalue. In general, SF is bounded by 1, but when σ is close to uniaxial, (or exactly uniaxial in the case of $\sigma = \sigma_{global}$) SF is bounded by ≈ 0.5. In Fig. 7 (b) the local Schmid factor for each individual twin was calculated based on the local stress tensor at the time and place of twin initiation. Lower ranked variants activate in all simulations, however in all cases twinning seems to be dominated by the variant of the highest Schmid factor. The dominance of the 1st rank variant is especially apparent in simulation *C*, where the twin stress relaxation rule was used. The variant rank distributions for simulations *A* and *B* are very similar regardless of the type of Schmid factor used whereas for *C* there is more difference between the distributions defined in the two ways.

5. Discussion

5.1. Discontinuous yielding

The results of the simulations show that the addition of the twin relaxation rule gives rise to a Lüders-like yield elongation. As the strain maps show, this is not an artefact of the twin stress relaxation rule (Eq. (2)) used in the simulations: the value of the scale parameter $g = 0.00002$ is two orders of magnitude smaller than the yield elongation in both simulations: $\varepsilon_L \approx 0.0016$ in *Set 1, C* and $\varepsilon_L \approx 0.0026$ in *Set 2, C*. This implies that the effect responsible for the yield elongation is, in fact, a collective phenomenon of twin relaxation triggering twins in neighbouring grains. If the stress drop involved in twin relaxation is sufficiently high and g sufficiently low, this triggering effect can produce long range correlations, leading to a macroscopic propagation effect, and a visible yield elongation. In this sense, the inclusion of twin relaxation in our model is a catalyst that allows for long range correlations to develop. The macroscopic effects of these correlations are, interestingly, rather insensitive to the details of the stress relaxation rule. To verify the twin propagation effect, we constructed "twin maps" for all the simulations taken at strains such that the overall fraction of twinned grains was the same, 0.16 in all cases (Fig. 8) The same regions are shown at the same applied strains in Fig. 4. We chose this scheme rather than plotting the maps at equal strains, so that we can compare the spatial organization of twinned IPs better. An IP is defined to have twinned significantly if its main variant has accumulated at least $\gamma_{twin} = 0.001$ of twinning shear. IPs that have twinned significantly are represented by a yellow square. Significantly twinned IPs appear to be scattered randomly for both simulations *A* and *B* in *Set 1*. Some clustering can be seen in *Set 1, C*, clearly as a consequence of the twin relaxation. Significantly twinned IPs appear to form small clusters in simulations *A* and *B* in *Set 2*. That simulations in *Set 2* appear to be more susceptible to twin clustering than those of *Set 1*, can be understood in the following way. When all IPs have different orientations, the system behaves more rigidly, as seen in the higher flow stress in the simulations of *Set 1*. In this case the presence of hard IPs acts to effectively shield softer grains (ones with high Schmid factor for twinning) from stress concentrations arising due to twin relaxation in the neighbourhood, hence hindering the overall average triggering effect. The shielding effect of hard IPs is less effective in the simulations of *Set 2*, where the system has more freedom to relax local stress concentrations. As a consequence, simulation *C* in *Set 2* shows a high degree of clustering. In this case, twinning appears to be emanating from one side of the sample, a vaguely defined propagation front

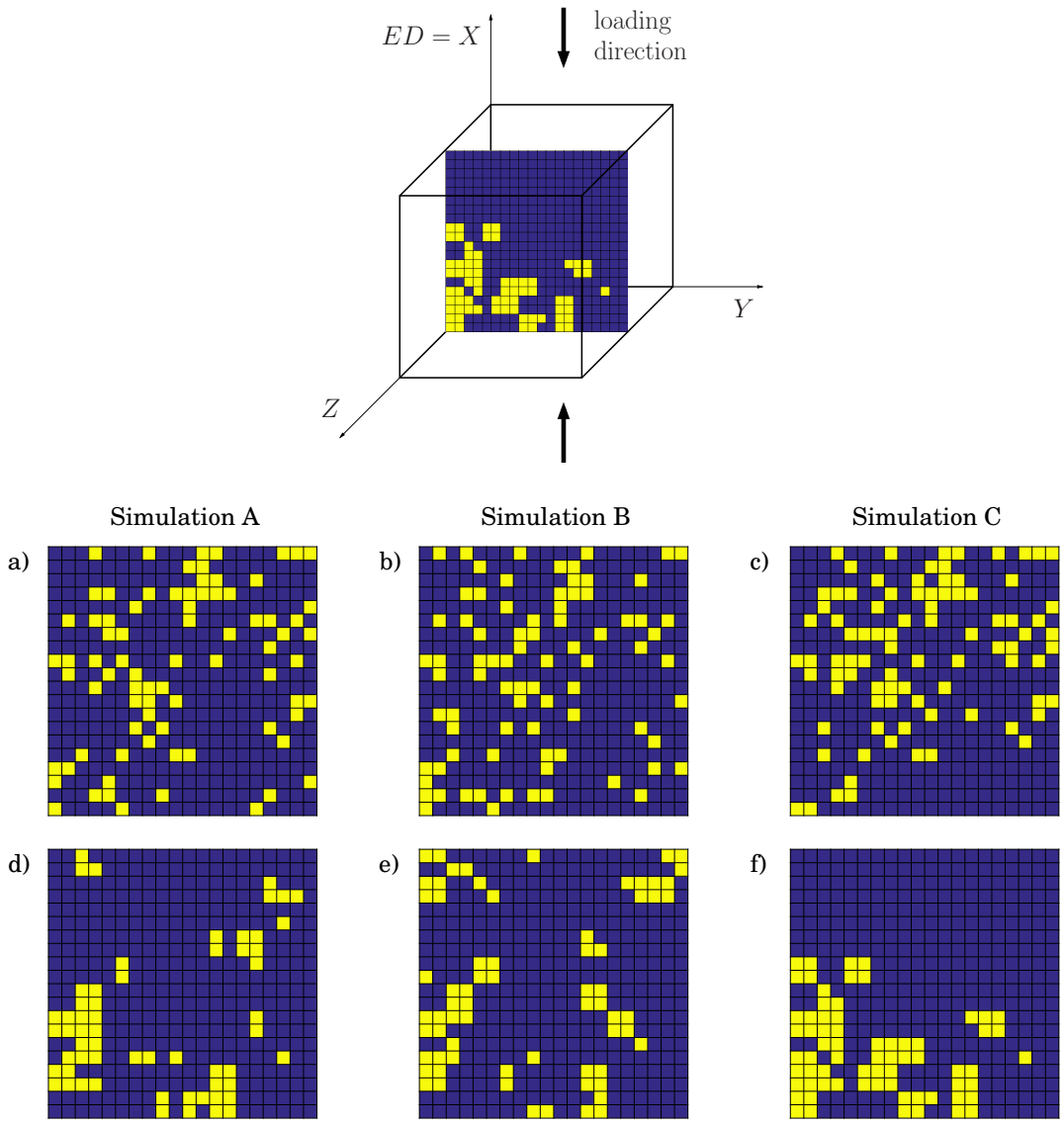

Figure 8: Twin maps for the XY plane cross section (see schematic diagram) for all three simulations in Set 1 *(a, b, c)* and Set 2 *(d, e, f)*. Yellow squares represent significantly twinned IPs, blue squares represent IPs that have not yet twinned significantly. The same regions are shown at the same applied strains in Fig. 4.

can be seen, similar to the Lüders-like propagation of twinning reported in [3].

This is clear indication of a strong local effect: on average, twinned grains will experience a compressive stress originating from the neighbourhood, as a reaction to the stress relaxation accompanying the twinning. Since we do not have geometrically defined twins in our model, the above mechanism is to be understood in an average sense; the IPs surrounding a twinned IP correspond to the "parent" material surrounding a twin in reality. It is these neighbouring IPs that, on average, experience an increasing compressive strain on the $\{0\,0\,0\,2\}$ and $\{1\,0\,\bar{1}\,3\}$ plane families, as twinning propagates along the sample. The fact that this strain reversal occurs so suddenly indicates a collective phenomenon of twins triggering twins in neighbouring grains, as suggested in [3]. This starts happening at ≈ 0.0017 applied strain, when stress concentrations begin to dominate new twin initiations, i.e. a propagation front evolves. This process elongates the twin initiation regime. Interestingly, the drop in twin initiation frequency for simulation *C* compared to *A* can be mainly attributed to the decrease of the activation of second, third, etc. variants in a given IP, as the frequency of first twin initiation stays approximately at the same level for simulations *A* and *C*.

5.2. Local stress distributions and twin variant selection

The different yielding behaviours will give rise to different local stresses during deformation, which in turn will affect the twin variants that are activated. One would expect the simulations that show yield elongation to have the highest local stress variation and therefore to show the largest amount of twinning in variants with low global Schmid factors. Surprisingly, the opposite happens: simulation *C* shows the lowest fraction of low ranked variants, particularly when the local Schmid factor is used in the ranking. To understand this counterintuitive finding, we need to look at the local stresses during yielding in more detail.

In Fig. 9 we plotted the distributions of twin resolved shear stresses at various stages of yielding. More specifically, Figure 9 shows the distribution of normalized resolved shear stresses $RSS/(m\sigma_{appl.})$ where RSS is the resolved shear stress (calculated using the local stress tensor) on a given twin variant and m is the global Schmid factor of the given variant. Only the three most heavily stressed twin systems were considered, and only IPs, that have not yet twinned significantly, i.e. where the accumulated twinning shear on the dominant variant is less than 0.001. The distributions were calculated at the following three different applied strains. Stage I: $\varepsilon = 0.0005$ (elastic region), Stage II: $\varepsilon = 0.0015$ (basal slip region) and Stage III: $\varepsilon = 0.003$ (twinning region).

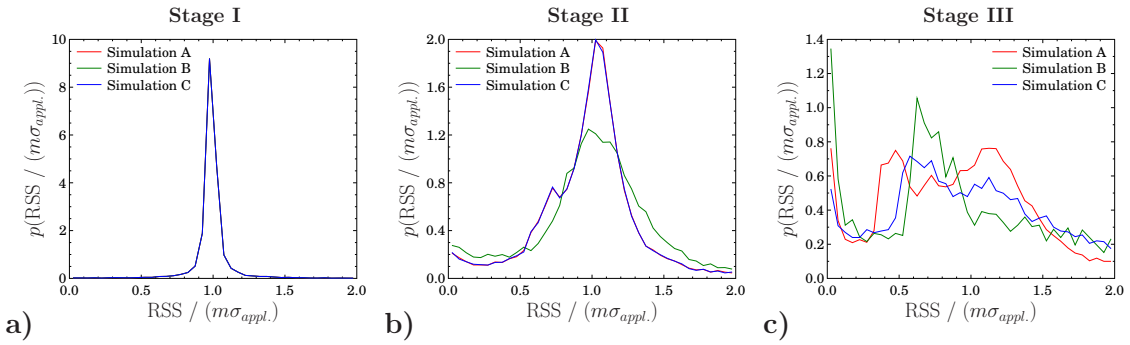

Figure 9: Distributions of normalized resolved shear stresses on the three most heavily stressed twin systems in IPs that have not yet twinned significantly. The parameter m is the global Schmid factor of the given twin variant. Applied strains for the three stages of deformation were as follows. Stage I: $\varepsilon = 0.0005$, Stage II: $\varepsilon = 0.0015$ and Stage III: $\varepsilon = 0.003$.

In the elastic region (Fig. 9 (a)), the resolved shear stress on virtually all twin systems equals that based on the global stress (averaged over all IPs). The small variance in this case is purely a consequence of the elastic anisotropy, which is very low for magnesium. The standard deviation of the distribution in the elastic region is the same for all three simulations: $std_A = std_B = std_C \approx 0.142$.

After microyielding by basal slip (Fig. 9 (b)) resolved shear stresses show considerably more deviation from their globally expected values: $std_A = std_C \approx 0.326$ and $std_B \approx 0.392$. The variance in the case of simulation B is slightly higher than that for simulations A and C, as twinning has already started in simulation B due to the lower twinning CRSS. In fact, $\approx 65\%$ of all twins in simulation B have already initiated by an applied strain of $\varepsilon = 0.0015$. In spite of this, the variance in the distribution for simulation B is only slightly higher than that for the other two simulations. The main reason for this is that even though a large fraction of the twins in simulation B have already initiated, they are still small in size, therefore have not contributed significantly to altering the globally enforced stress state.

At Stage III, when most twins have already initiated in all three simulations, and have already contributed considerably to the global plastic strain, the stress distributions become wider: $std_A \approx 0.466$, $std_B \approx 0.531$ and $std_C \approx 0.499$. Although the stress distributions are different for the different cases, the variance is similar. Also, the standard deviation for simulation C is only slightly higher than that for simulation A, and lower than that for B even at this late stage. Based on these results one would not expect a great difference between the three simulations in terms of how active twin variant ranks are distributed. This explains why

the variant rank distributions of A and B are indeed similar, as can be seen in in Fig. 7. This is not the case for simulation C, however; the noticable difference between global and local Schmid factor, in this case, indicates that there are higher stress fluctuations in the system (at the time and place of twin initiations!) compared to that of simulations A and B.

Recalling Fig. 9 where we saw that the variance in resolved shear stress is more or less the same for all simulations (in fact, the variance for simulation C was found to be between that of the other two simulations) we can arrive at the following conclusion. The excessive stress fluctuations at twin initiation in simulation C, inferred from the variant rank distributions, are only present in a relatively small fraction of the system volume at any given stage of deformation. In simulation C most twins initiate at the propagation front (see Fig. 8 (f)) and indeed this is the only region in the system that has high stress fluctuations. The stress field in the rest of the system volume is not much more heterogeneous than it is for the other two simulations. One should note here that the activation of lower ranked variants in itself is not necessarily a sign of stress fluctuations: mean field models also predict lower rank variants to be active. A better indicator of stress fluctuations is the difference of twin variant selection based on global and local Schmid factor. It is therefore entirely plausible that simulation C has higher stress fluctuations at twin initiation compared to A and B, and at the same time has a more dominant first variant in the variant rank distributions. In this spirit we can understand the coexistance of the two seemingly contradictory phenomena: Lüders-like propagation of twinning (requiring the presence of stress fluctuations) and "well-behaved" twin variant rank distributions. To shed some further light on how stress heterogeneity influences twinning, and to reinforce our above reasoning, it is informative to plot the distribution of the maximum (among all variants) global Schmid factor for twinned and untwinned IPs. In Fig. 10 we plotted these distributions for two stages of deformation: at an applied strain of $\varepsilon = 0.003$ (Fig. 10 (a)), which is in the twin propagation regime, and an applied strain of $\varepsilon = 0.02$ (Fig. 10 (b)), at the end of the simulation.

In the propagation regime we see that mainly only high maximum Schmid factor IPs twin in all three simulations. This is especially true for simulation C. As expected, untwinned IPs mostly have small maximum Schmid factors, but apparently, in all the simulations, there remain untwinned IPs that had high maximum Schmid factors. The fraction of such IPs is especially high in the case of simulation C. This is easily understood: as twinning occurs along a propagation front, the IPs not yet visited by the propagation, in general,

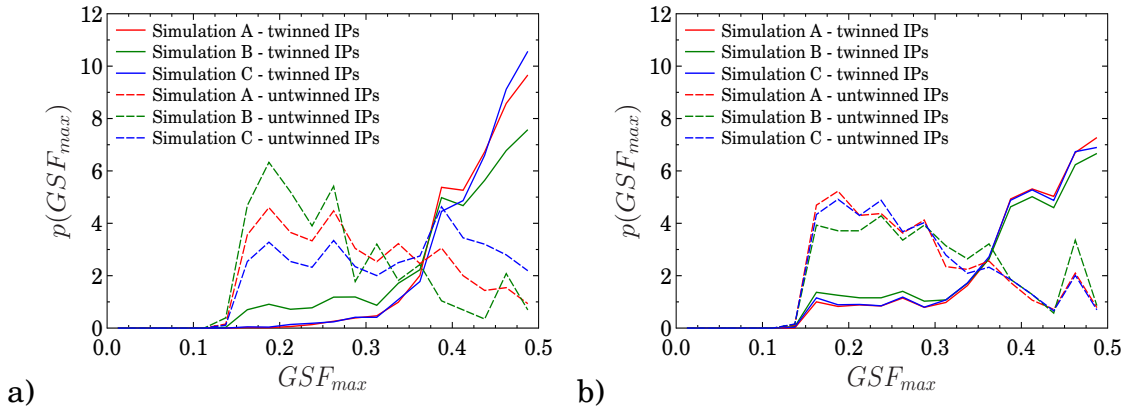

Figure 10: Distribution of maximum global Schmid factor for twinned and untwinned IPs. The distributions were calculated at applied strains of $\varepsilon = 0.003$ *(a)* and $\varepsilon = 0.02$ *(b)*.

do not twin regardless of their high maximum Schmid factor. For simulations *A* and *B*, there is no such propagation, twinning occurs in a more homogeneous, diffuse manner, therefore high maximum Schmid factor IPs are likely to twin first. Looking at the same distributions at the end of the simulation, we see that, interestingly, there is very little difference between the three simulations regarding both the twinned and untwinned IPs. At this stage the twin propagation front in simulation *C* has already moved over the entire sample, all IPs of high maximum Schmid factors have twinned.

A significant difference that is still observable at the end of the simulations is in the distribution of twinning shear among the active variants within a single IP. Figure 11 shows twin variant rank distributions based on accumulated twinning shear rather than Schmid factor, for the same two values of applied strain as in Fig. 10. We see that in the propagation regime, virtually all twinning shear occurs on the main variant in simulation *C*, whereas in simulations *A* and *B*, the second variant also bears a considerable fraction of the total shear. The distribution of twinning shear for these two cases is almost exactly the same at the end of the simulation. The dominance of the first variant in simulation *C* decreases slightly, but is still considerable at $\varepsilon = 0.02$. This decrease is due to the more diffuse twinning occurring after the propagation front has passed. This clear dominance of the first variant in terms of twinning shear in simulation *C* corresponds well to the "one twin per grain" condition for twin propagation established in [3]. Although it should be noted that our model cannot distinguish between different twins of the same variant, so this correspondence is not perfect; in our case we can only talk about "one variant per grain". Multiple variants would, however, definitely

mean multiple twins, therefore our "one variant per grain" condition still provides support for the "one twin per grain" situation of [3].

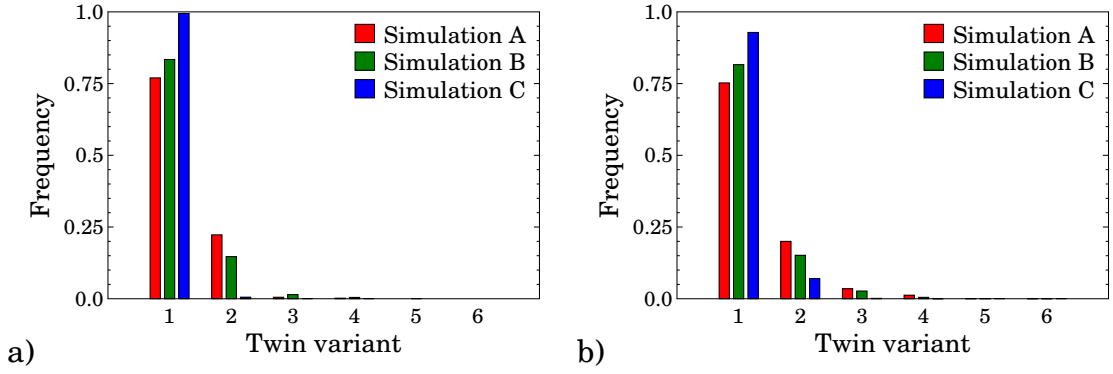

Figure 11: Twin variant rank ditributions based on total accumulated twinning shear. The distributions were calculated at applied strains of $\varepsilon = 0.003$ *(a)* and $\varepsilon = 0.02$ *(b)*.

Finally we briefly discuss the question of how the heterogeneity of the stress field throughout the sample is affected by the magnitude of the twinning stress and the twin stress relaxation assumption. Figure 12 shows the average von Mises stress (*a*), the standard deviation in von Mises stress (*b*) and the relative standard deviation in von Mises stress (*c*) as a function of true strain (average axial true strain).

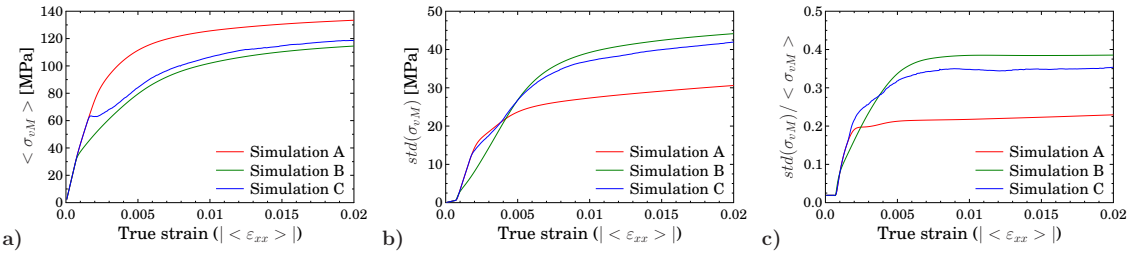

Figure 12: Average von Mises stress *(a)*, standard deviation in von Mises stress *(b)* and relative standard deviation in von Mises stress *(c)*, as functions of applied strain.

It is interesting to note that in spite of the stress relaxation rule, the standard deviation of von Mises stress in Simulation *C* never exceeds the maximum of Simulation *A* and *B*. Initially, $std(\sigma_{vM})_C$ ($std(\sigma_{vM})$ for simulation *C*) increases together with $std(\sigma_{vM})_A$, as both have high initiation stresses for twinning. After the twin propagation front appears, at ≈ 0.0017, $std(\sigma_{vM})_C$ increases slightly slower than $std(\sigma_{vM})_A$. The reason

for the slower increase is, that even though the propagation front has higher stress fluctuations, the average stress and therefore the standard deviation in stress in the rest of the system is lower compared to simulation *A*. This continues until an applied strain of ≈ 0.004, by which the twin propagation front has passed over the entire sample. (During this propagation regime the relative standard deviation of stress in simulation *C* is higher, because the global stress is reduced significantly by the Lüders effect, while in most of the sample the heterogeneity of the stress field still resembles that of simulation *A*.) From this point onward the evolution of the stress field is regulated mainly by the growth of existing twins. Keeping in mind, that most existing twins in simulation *C* now have a low propagation stress, it is not surprising that $std(\sigma_{vM})_C$ starts following the curve for $std(\sigma_{vM})_B$ after this transition point. After this point, it is mainly the ratio of CRSS values (asymptotic ratio in the case of simulation *C*) for the different deformation modes that determine $std(\sigma_{vM})$. Large differences in the CRSS for twinning and prismatic slip in the case of simulation *B* and *C* lead to higher $std(\sigma_{vM})$ than $std(\sigma_{vM})_A$. Interestingly, after the transition point, $std(\sigma_{vM})_C$ increases slower than $std(\sigma_{vM})_B$, even though practically all active twins in these two simulations propagate at the same low stress, 15 MPa, after an applied strain of ≈ 0.004. This can be qualitatively understood in the following sense. After the Lüders front has passed through in simulation *C*, the scenario established is such that there is approximately one well aligned (high Schmid factor) active twin in every IP, whereas in simulation *B* the situation is more "random": there are more than one active twins, some of which are not very well aligned. The "one twin per grain" situation regulates the stress field more efficiently after the transition, leading to smaller average fluctuations in von Mises stress.

6. Conclusions

We investigated the yielding behaviour of extruded magnesium in uniaxial compression, concentrating on the role of $\{1\,0\,\bar{1}\,2\}\ \langle 1\,0\,1\,1\rangle$ tensile twinning. Using the twin stress relaxation rule we were able to reproduce the yield point elongation in the stress strain curves seen in experiments. In the simulations, a twin propagation effect, similar to a Lüders-like band propagation, could be observed.

Our results reinforce the ideas presented in [2, 3] whereby the phenomenon of yield point elongation and the associated twin propagation are a consequence of twin stress relaxation: the sudden decrease of twinning stress produces stress concentrations in the neighbouring grains and therefore, may trigger twins

in these neighbouring grains.

Our simulations could also predict the strain reversal in $\{0\,0\,0\,2\}_{\perp}$ and $\{1\,0\,\bar{1}\,3\}_{\perp}$ grain families, which has been observed in conjunction with the above mentioned phenomena in magnesium. The EPSC model has failed to account for this strain reversal effect, which implies that stress fluctuations due to twinning, simulated in the CPFEM, are likely to play a major role.

Using the twin stress relaxation rule, the total twinning shear is dominated by the first activated variant at IPs, while a constant CRSS for twinning resulted in more variants contributing to the total shear. The dominance of the first variant, in the simulation using the twin stress relaxation rule, corresponds well to the "one twin per grain" condition found in [3].

The simulations showed that the twin relaxation rule does not introduce significant fluctuations in the resolved shear stresses on twin systems in the majority of IPs because twinning occurs mainly along a propagation front.

The propagation of tensile twins in magnesium, and the consequent evolution of an approximate "one twin per grain" microstructure may be important in many deformation processes, where conditions are right for profuse tensile twinning. Understanding the formation of mesoscopic twin structures based on the initiation and growth properties of the different twin types, is vital for an accurate prediction of the macroscopic deformation behaviour and formability of magnesium alloys.

Acknowledgements

The authors gratefully thank EPSRC for funding this work through programme grant EP/H020047/1, Light Alloys for Sustainable Transport (LATEST2). G. Timár acknowledges support from the FET proactive IP project MULTIPLEX 317532.

References

[1] M. R. Barnett, A. Ghaderi, J. D. Robson, Contribution of twinning to low strain deformation in a Mg alloy, Metallurgical and Materials Transactions A 45 (8) (2014) 3213–3221.

[2] O. Muránsky, M. Barnett, V. Luzin, S. Vogel, On the correlation between deformation twinning and Lüders-like deformation in an extruded Mg alloy: In situ neutron diffraction and EPSC. 4 modelling, Materials Science and Engineering: A 527 (6) (2010) 1383–1394.

[3] M. R. Barnett, M. D. Nave, A. Ghaderi, Yield point elongation due to twinning in a magnesium alloy, Acta Materialia 60 (4) (2012) 1433–1443.

[4] Y. Pei, A. Godfrey, J. Jiang, Y. Zhang, W. Liu, Q. Liu, Extension twin variant selection during uniaxial compression of a magnesium alloy, Materials Science and Engineering: A 550 (2012) 138–145.

[5] L. Capolungo, P. Marshall, R. McCabe, I. Beyerlein, C. Tomé, Nucleation and growth of twins in Zr: a statistical study, Acta Materialia 57 (20) (2009) 6047–6056.

[6] I. Beyerlein, L. Capolungo, P. Marshall, R. McCabe, C. Tomé, Statistical analyses of deformation twinning in magnesium, Philosophical Magazine 90 (16) (2010) 2161–2190.

[7] I. Beyerlein, R. McCabe, C. Tomé, Effect of microstructure on the nucleation of deformation twins in polycrystalline high-purity magnesium: a multi-scale modeling study, Journal of the Mechanics and Physics of Solids 59 (5) (2011) 988–1003.

[8] C. Tomé, I. Beyerlein, J. Wang, R. McCabe, A multi-scale statistical study of twinning in magnesium, JOM 63 (3) (2011) 19–23.

[9] M. Barnett, A. Ghaderi, J. Q. da Fonseca, J. Robson, Influence of orientation on twin nucleation and growth at low strains in a magnesium alloy, Acta Materialia 80 (2014) 380–391.

[10] H. Abdolvand, M. R. Daymond, Multi-scale modeling and experimental study of twin inception and propagation in hexagonal close-packed materials using a crystal plasticity finite element approach; part II: Local behavior, Journal of the Mechanics and Physics of Solids 61 (3) (2013) 803–818.

[11] H. Qiao, M. Barnett, P. Wu, Modeling of twin formation, propagation and growth in a Mg single crystal based on crystal plasticity finite element method, International Journal of Plasticity 86 (2016) 70–92.

[12] E. Hall, Yield point phenomena in metals and alloys, Springer Science & Business Media, 2012.

[13] J. Wyrzykowski, M. Grabski, Lüders deformation in ultrafine-grained pure aluminium, Materials Science and Engineering 56 (2) (1982) 197–200.

[14] N. Ecob, B. Ralph, The effect of grain size on deformation twinning in a textured zinc alloy, Journal of Materials Science 18 (8) (1983) 2419–2429.

[15] R. E. Reed-Hill, R. Abbaschian, Deformation twinning and martensite reactions, Physical Metallurgy Principles (1998) 584–585.

[16] P. Sittner, Y. Liu, V. Novák, On the origin of Lüders-like deformation of NiTi shape memory alloys, Journal of the Mechanics and Physics of Solids 53 (8) (2005) 1719–1746.

[17] B. Clausen, C. Tomé, D. Brown, S. Agnew, Reorientation and stress relaxation due to twinning: modeling and experimental characterization for Mg, Acta Materialia 56 (11) (2008) 2456–2468.

[18] S. Agnew, D. Brown, C. Tomé, Validating a polycrystal model for the elastoplastic response of magnesium alloy AZ31 using in situ neutron diffraction, Acta Materialia 54 (18) (2006) 4841–4852.

[19] O. Muránsky, D. Carr, M. Barnett, E. Oliver, P. Šittner, Investigation of deformation mechanisms involved in the plasticity of AZ31 Mg alloy: In situ neutron diffraction and EPSC modelling, Materials Science and Engineering: A 496 (1) (2008) 14–24.

[20] Y. Chun, C. Davies, Texture effect on microyielding of wrought magnesium alloy AZ31, Materials Science and Engineering: A 528 (9) (2011) 3489–3495.

[21] R. Lebensohn, C. Tomé, A self-consistent anisotropic approach for the simulation of plastic deformation and texture development of polycrystals: application to zirconium alloys, Acta Metallurgica et Materialia 41 (9) (1993) 2611–2624.

[22] S.-H. Choi, E. Shin, B. Seong, Simulation of deformation twins and deformation texture in an AZ31 Mg alloy under uniaxial compression, Acta Materialia 55 (12) (2007) 4181–4192.

[23] D. Brown, S. Agnew, M. Bourke, T. Holden, S. Vogel, C. Tomé, Internal strain and texture evolution during deformation twinning in magnesium, Materials Science and Engineering: A 399 (1) (2005) 1–12.

[24] S.-B. Yi, C. Davies, H.-G. Brokmeier, R. Bolmaro, K. Kainer, J. Homeyer, Deformation and texture evolution in AZ31 magnesium alloy during uniaxial loading, Acta Materialia 54 (2) (2006) 549–562.

[25] G. Proust, C. Tomé, G. Kaschner, Modeling texture, twinning and hardening evolution during deformation of hexagonal materials, Acta Materialia 55 (6) (2007) 2137–2148.

[26] J. Q. Da Fonseca, E. Oliver, P. Bate, P. Withers, Evolution of intergranular stresses during in situ straining of IF steel with different grain sizes, Materials Science and Engineering: A 437 (1) (2006) 26–32.

[27] P. Bate, J. Q. da Fonseca, Texture development in the cold rolling of IF steel, Materials Science and Engineering: A 380 (1) (2004) 365–377.

[28] G. Timár, J. Q. da Fonseca, Modeling twin clustering and strain localization in hexagonal close-packed metals, Metallurgical and Materials Transactions A 45 (13) (2014) 5883–5890.

[29] K. M. Krishna, D. L. Prakash, G. Timár, A. Fitzner, D. Srivastava, N. Saibaba, J. Q. da Fonseca, G. Dey, M. Preuss, The effect of loading direction and Sn alloying on the deformation modes of Zr: An in-situ neutron diffraction study, Materials Science and Engineering: A 650 (2016) 497–509.

[30] P. Bate, Modelling deformation microstructure with the crystal plasticity finite–element method, Philosophical Transactions of the Royal Society of London. Series A: Mathematical, Physical and Engineering Sciences 357 (1756) (1999) 1589–1601.

[31] D. Tromans, Elastic anisotropy of HCP metal crystals and polycrystals, Int. J. Res. Rev. Appl. Sci 6 (4) (2011) 462–483.

[32] M. A. Gharghouri, G. C. Weatherly, J. D. Embury, J. Root, Study of the mechanical properties of Mg-7.7at.% Al by in-situ neutron diffraction, Philosophical Magazine A 79 (7) (1999) 1671–1695.

[33] S. Agnew, C. Tomé, D. Brown, T. Holden, S. Vogel, Study of slip mechanisms in a magnesium alloy by neutron diffraction and modeling, Scripta Materialia 48 (8) (2003) 1003–1008.

[34] O. Muránsky, D. G. Carr, P. Šittner, E. C. Oliver, In situ neutron diffraction investigation of deformation twinning and pseudoelastic-like behaviour of extruded AZ31 magnesium alloy, International Journal of Plasticity 25 (6) (2009) 1107–1127.

[35] C. Mareau, M. R. Daymond, Micromechanical modelling of twinning in polycrystalline materials: Application to magnesium, International Journal of Plasticity 85 (2016) 156–171.